JOURNAL OF MATERIALS SCIENCE 35 (2000) 5319–5329

Evaluation of volume fraction of solid in alloys formed by semisolid processing

E. TZIMAS*‡, A. ZAVALIANGOS
Department of Materials Engineering, Drexel University, Philadelphia PA 19104, USA
E-mail: tzimas@jrc.nl

Three of the methods used to determine the volume fraction of solid as a function of temperature in alloys in the semisolid state, namely utilization of thermodynamic data, thermal analysis, and quantitative metallography on quenched microstructures, are studied. The accuracy of each method is evaluated and the advantages and limitations are recognized. It is demonstrated that, while all methods are approximate, they offer distinct and different advantages.

1. Introduction

Increased interest in semisolid metal processing during the recent years has created the need for the accurate evaluation of the volume fraction of solid in semisolid alloys as a function of temperature, since this parameter controls to a large extent the rheological behavior [1–5] and the evolution of microstructure [6–11] in the semisolid state. Thus, this parameter is of critical importance, both for fundamental work and for the control of the process. It is important to note that, for each alloy, the volume fraction of solid is defined uniquely at a given temperature only under equilibrium conditions. In any other case, it depends on the prior thermal history.

The volume fraction of solid, g_S, can be evaluated either directly or through its effects on a physical property. The following methods are potential candidates:

- utilization of thermodynamic data (equilibrium phase diagrams),
- thermal analysis techniques,
- quantitative metallography on microstructures quenched from the semisolid state,
- ultrasonic monitoring (measurement of propagation speed of ultrasonic waves),
- measurement of electrical resistance/magnetic permeability, and,
- measurement of mechanical response (by indentation, back extrusion etc.).

The last three methods not only require calibration but there is no unique correspondence between the characteristic parameter measured (ultrasonic wave velocity ratio, average electrical resistance, and resistance to deformation respectively) and the volume fraction of solid. This is because, wave propagation and the electrical, magnetic and mechanical properties of semisolid alloys depend strongly on the microstructure as well, especially on the connectivity and distribution of the solid phase. For these reasons, in this paper we focus our attention on the first three methods. Use of phase diagrams, thermal analysis, and image analysis are described and examined below in terms of accuracy and ability to characterize the transient states typical of industrial implementations of semisolid processing. For this reason, we draw examples from our work on the characterization of semisolid microstructures [12]. We evaluate the volume fraction of solid in wrought and cast aluminum alloys that have been produced by the three major methods used for the production of alloys with near-equiaxed microstructure, that are suitable for subsequent semisolid processing: spray casting, magnetohydrodynamic (MHD) casting, and the stress induced, melt activated (SIMA) process [1, 2]. Alloys produced by these three methods share a similar thermal history: they are produced from complete solidification of the liquid phase but under different conditions; during semisolid processing they are reheated with very high heating rates and soaked for short periods of time (of the order of few minutes) in the semisolid state prior to forming.

2. Experimental procedures

Wrought and cast aluminum alloys, produced by spray-casting, MHD-casting and the SIMA process, were examined by thermal analysis and quenching experiments. The most common alloys in semisolid forming, the Al-7wt.%Si hypoeutectic alloys were the main alloys investigated. In this work, Al-7.2wt.%Si alloys produced by spray casting and SIMA were compared with a A356 MHD-cast alloy. In addition, spray-cast Al-4wt.%Cu and 2014 alloys were also investigated. Spray-cast preforms of Al-4wt.%Cu, 2014

* Author to whom all correspondence should be addressed.
‡ *Present Address*: European Commission – Joint Research Centre, Institute for Advanced Materials, P.O. Box 2, 1755 ZG, Petten, The Netherlands.

TABLE I Chemical composition (in wt.%) of alloys studied

Alloy Element	Spray-Cast / SIMA Al-7.2wt.%Si	MHD-Cast A356	Spray-Cast 2014	Spray-Cast Al-4wt.%Cu
Cu	<0.05	<0.05	4.24	4.04
Si	7.16	6.89	0.74	0.05
Mg	<0.05	0.32	0.61	<0.05
Fe	0.21	0.12	0.39	0.09
Ti	<0.05	<0.05	<0.05	<0.05
Zn	<0.05	<0.05	0.23	<0.05
Mn	0.09	<0.05	0.77	<0.05
Pb	<0.05	<0.05	<0.05	<0.05
Sn	<0.05	<0.05	<0.05	<0.05
Ni	<0.05	<0.05	<0.05	<0.05
Cr	<0.05	<0.05	<0.05	<0.05
Al	balance	Balance	balance	balance

and Al-7.2wt.%Si were provided by Osprey Metals Ltd., Neath, UK. MHD-cast A356 was provided by CTC, Johnstown, PA, in the form of cylindrical ingots, 7.62 cm in diameter (3″). SIMA Al-7.2wt.%Si was produced in the laboratory. Details on the process of producing the SIMA alloy can be found in [11, 12]. The chemical composition of the alloys used in this work is shown in Table I.

2.1. Determination of volume fraction of solid using thermal analysis

Thermal analysis techniques have been used traditionally in order to evaluate the weight fraction of solid [13–17]. The procedure consists of three steps: initially, the heat of melting is measured, and subsequently, the weight fraction of solid is calculated using the *method of partial areas.* Finally, the results for the weight fraction of solid are transformed into volume fraction of solid.

Differential scanning calorimetry (DSC) has an advantage compared with differential thermal analysis (DTA), as it measures directly the evolution of the heat of melting during the solid-liquid phase transformation, especially with the recent development of high temperature DSC instruments that permit measurements to temperatures up to 1700°C. In this method, small pieces of the alloy under investigation, ∼5 mg, are heated from a temperature where the alloy is 100% solid (usually 30°C below the nominal solidus temperature[§]), to a temperature above the liquidus. The result is given in terms of the differential power flow rate, $(\mathrm{d}Q/\mathrm{d}t)$, required by the specimen in order to be at the same temperature with a reference sample, as a function of temperature, when heated at a constant heating rate. The energy absorbed during heating contributes to the change of the heat content of the solid and liquid phases and the heat of melting [18, 19]:

$$\frac{\mathrm{d}Q}{\mathrm{d}t} = m\left(f_\mathrm{s}C_{\mathrm{p,s}} + (1 - f_\mathrm{s})C_{\mathrm{p,L}} + \Delta H \frac{\mathrm{d}\,f_\mathrm{s}}{\mathrm{d}T}\right)\frac{\mathrm{d}T}{\mathrm{d}t} \quad (1)$$

[§] The solidus temperature is herein used in a broader sense as the temperature where the first liquid phase is formed, thus substituting for the eutectic temperature.

where m is the mass of the sample, $C_{\mathrm{p,S}}$ and $C_{\mathrm{p,L}}$ are the heat capacities of the solid and liquid phases respectively, and, ΔH is the heat of melting.

To simplify the calculations, a baseline is defined, used to isolate the energy that corresponds to the heat of melting of the solid phase and thus the term $\mathrm{d}\,f_\mathrm{s}/\mathrm{d}T$, from the heat needed to change heat content. Although a straight line may be adequate when the heat capacities of the solid and liquid phases do not vary significantly, typically a sigmoidal baseline must be created to define the lower limit of the area under the DSC curve. This is necessary since the slope of the baseline (which represents the heat capacity) changes with a phase transformation, and the use of a linear baseline may lead to significant errors. The simplest method to create the sigmoidal baseline is the extrapolation of the initial and final baselines to the thermodynamic transformation temperature. This method is approximate and may introduce errors in the results. More accurate methods require the knowledge of the exact values of heat capacities of the solid and liquid phases [20]. The total area between the DSC curve and the created baseline corresponds to the net energy required to melt the sample, the heat of melting.

Since measurements are performed at a fixed heating rate, $\dot{T}$, the decrease of the weight fraction of solid during melting can be calculated from the measured increase of the absorbed heat of melting. From Equation 1:

$$\begin{aligned}\mathrm{d}\,f_\mathrm{s} &= \frac{1}{\dot{T}m\Delta H}\left(\frac{\mathrm{d}Q}{\mathrm{d}t}\right)\mathrm{d}T \Leftrightarrow \Delta f_\mathrm{s} = 1 - f_\mathrm{s}(T) \\ &= \frac{1}{\dot{T}m}\int_{T_\mathrm{S}}^{T}\frac{1}{\Delta H}\left(\frac{\mathrm{d}Q}{\mathrm{d}t}\right)\mathrm{d}T \end{aligned} \quad (2)$$

A usual approximation to Equation 2 is derived by assuming that, *the heat of melting is independent of the temperature and thus the composition of the solid phase and is linearly proportional to the amount of the melted alloy:*

$$f_\mathrm{s}(T) = 1 - \frac{1}{m\Delta H}Q(T) \quad (3)$$

where $Q(T)$ is the heat absorbed from the beginning of melting until the temperature of the alloy is T, or in other words the area under the DSC curve bound on the right by the temperature of interest. Then, the weight fraction of solid is proportional to the evolution of heat during melting, i.e. the area under the DSC curve. This approach is called the *method of partial areas.* The transformation of the weight content into volume content is described in 3.1.

Our experiments were performed with a heating rate of 10 K/min using a Perkin Elmer DSC 7. Small samples were machined from the billets of the examined alloys and tested using alumina holders. Samples were taken from various positions from each ingot to minimize the possibility of getting non-representative results due to local compositional variations due to segregation. Our results showed that, the melting behavior

in spray-cast alloys did not vary with the position of the ingot where the tested samples came from, while the variation observed when the SIMA and MHD-cast alloys were tested was small, within the experimental error of the method.

2.2. Determination of volume fraction of solid using quenching experiments

Quenching experiments are used to 'freeze' the microstructure in the semisolid state and permit the evaluation of the volume fraction of solid using quantitative metallography. The cooling rate during quenching has to be very fast to minimize the extent of dendritic and epitaxial solidification of liquid on the solid phase, which increases the size of the solid grains and reduces the accuracy of the method.

Image analysis is used to calculate the volume fraction of solid from images of the quenched microstructure, typically obtained by optical microscopy. The method consists of four discrete steps: sample selection and preparation, image acquisition and processing, measurement and data analysis [21]. The area selected for analysis from the quenched sample must be representative for the alloy. Examination of microstructure of semisolid alloys has shown that, although the solid phase is uniformly distributed in the liquid phase in SIMA and spray-cast alloys, it exhibits a high degree of segregation in MHD-cast alloys [11]. Therefore, a large area has to be examined in order to obtain representative and reproducible results. Typically, many areas from the same sample have to be measured. These areas must be selected based on a systematic sampling plan to minimize the bias from the operator. Samples must be prepared very carefully: an image of good quality, a result of proper polishing and etching that enhances contrast between the solid and liquid phases, permits the unambiguous detection and identification of the phases by the image analyzer. Bad image quality from preparation and focusing and uneven sample lighting introduces an error in the results. The two phases are distinguished by gray level thresholding that is performed either manually or automatically. Automatic thresholding minimizes the influence of operator fatigue, reduces the analysis time, and increases the accuracy and reproducibility of the measurements compared with manual thresholding. After the phases have been identified, the volume fraction of solid is calculated by the ratio of picture elements that correspond to the solid phase to the number of picture elements that correspond to the whole image.

The experimental setup designed to test the accuracy of the method is shown in Fig. 1a. A vertical tube furnace was used to heat the sample to the quenching temperature. The sample was hung inside the furnace by a thin copper wire. A calibrated thermocouple was placed inside a hole located on the top surface of the sample (3–4 mm deep) to ensure that the sample had reached the predefined quenching temperature. The material was heated to the quenching temperature with an average heating rate of 40 K/min and soaked for 2 min before quenching, to ensure uniform partial melting.

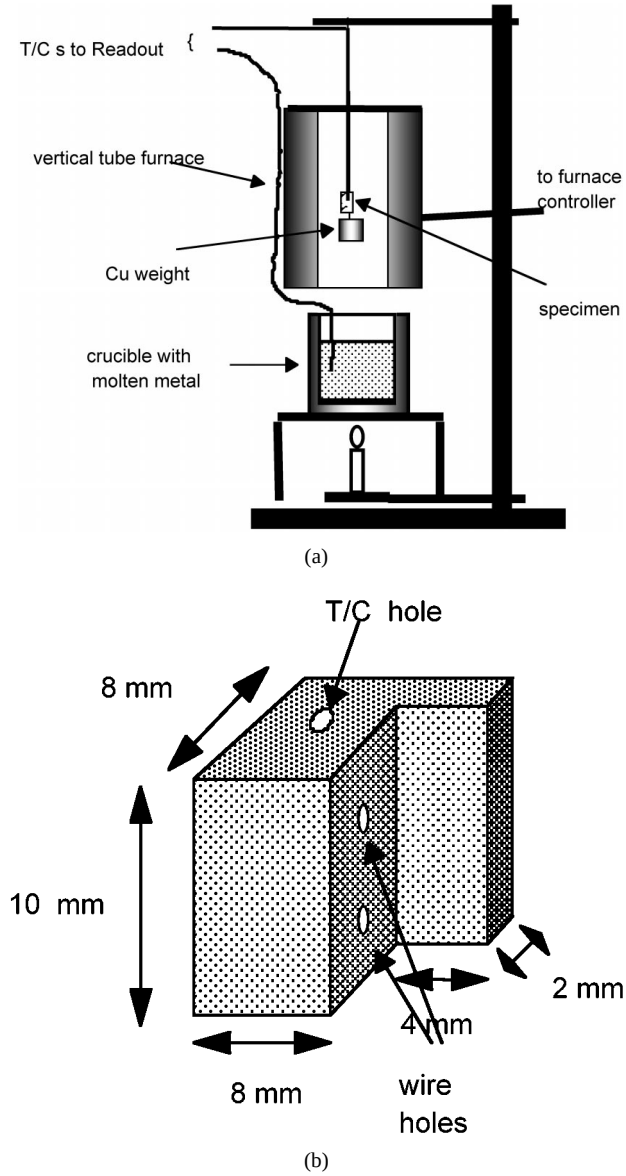

Figure 1 (a) Setup used for the quenching experiments; (b) quenching sample.

After soaking, the wire was cut and the specimen was immersed into the quencher. To ensure that the specimen is cooled rapidly, its dimensions must be kept to a minimum. On the other hand, the strength of the alloy is decreased at temperatures above solidus, so the presence of thick walls around the thermocouple hole is necessary to keep the thermocouple inside the specimen. To overcome this problem, L-shaped specimens were used, as shown in Fig. 1b. The thick part of the sample supported the thermocouple while the thin part was quenched rapidly and used for examination.

While water is usually been used as a quencher, liquid metal of low melting point was chosen as the quenching medium for our experiments. Quenching was done in liquid eutectic Sn-Pb (solder) that offers high thermal diffusivity and good wettability of the samples and eliminates the problem of reduced heat transfer due to the formation of a vapor film on the surface of the sample when water is used as the quencher. The quencher was placed underneath the furnace and was held at a temperature of $\sim$220°C using a gas torch. In order to

overcome the buoyancy of the specimens in the liquid solder (density 8.8 g/cm^3), a piece of copper (density 8.98 g/cm^3) was attached to the samples, dragging them into the bath. Relatively high cooling rates of the order of 70 K/s were achieved using this setup. An estimate was made by measuring the secondary dendrite arm spacing (SDAS) of the rapidly solidified liquid phase [22, 23]. The measured SDAS for the Al-Si and Al-Cu alloys were 2.5 μm and 4.3 μm respectively.

Images from the quenched microstructures were taken at relatively low magnification (100×–200×). Finally, the public domain NIH Image 1.55 software [24] was used to evaluate the volume fraction of solid.

3. Analysis

3.1. Calculation of volume fraction of solid utilizing thermodynamic data

Direct evaluation of the volume fraction of solid based on phase diagrams can be performed for alloys that melt or solidify under equilibrium conditions only. For simple binary eutectic alloys, the lever rule allows for the analytical determination of the weight fraction of solid, f_s^{Eq}, at a given temperature, T, in the semisolid range. Assuming that the solidus and liquidus lines of the phase diagram are linear then:

$$f_s^{Eq} = \frac{(T_M - T) - m_L C_0}{(T_M - T)(1-k)} \tag{4}$$

where k is the partition coefficient of the alloy, m_L is the slope of the liquidus line, C_0 is the alloy composition and T_M is the melting point of the pure solvent.

The phase diagram can also be used in the case of a fully microsegregated alloy that results from non-equilibrium solidification conditions, i.e. under complete diffusion in the liquid phase and no diffusion in the solid phase. For simple binary alloys, the non-equilibrium lever rule, or Scheil equation, can be used for the analytical determination of the weight fraction of solid, f_s^{Sch}, at a given temperature in the semisolid range [25]:

$$f_s^{Sch} = 1 - \left(\frac{T_M - T}{T_M - T_L}\right)^{-\frac{1}{1-k}} \tag{5}$$

where T_L is the liquidus temperature of the alloy.

Thermodynamic database software such as Thermocalc [26], can utilize equilibrium phase diagrams and the Scheil equation to allow for the prediction of the weight fraction of solid in complex multi-component alloy systems.

Finally, to determine the volume fraction of solid from the weight fraction of solid, it is necessary to know the densities of the solid and liquid phases, ρ_S and ρ_L respectively, as functions of temperature, T, and composition, C:

$$g_s = \frac{f_s}{f_s + (1 - f_s)\dfrac{\rho_s(C,T)}{\rho_L(C,T)}} \tag{6}$$

However, equilibrium and maximum microsegregation conditions represent limiting cases. Although non-equilibrium conditions are often present during solidification of alloys, slow back diffusion in the solid phase during and after solidification leads to homogenization of the solid phase. In addition, partial reheating prior to semisolid forming results in a further shift from microsegregated towards equilibrium conditions. Therefore, the extent of back diffusion determines the level of homogenization and furthermore, the solid content at a given temperature. Complex models, based on solute redistribution, are required to predict the evolution of solid during solidification and remelting that include back diffusion in the solid while the alloy is in the semisolid state [18, 25]. According to these models, the weight solid fraction in binary eutectic alloys is given as a function of the modified Fourier number of the process, a':

$$f_s = \frac{1}{1 - 2\alpha' k}\left\{1 - \left[\frac{T_M - T}{m_L C_0}\right]^{\frac{1-2\alpha' k}{k-1}}\right\} \tag{7}$$

The modified Fourier number, a', is used to describe the thermal history of the alloy, and is of the form [18]:

$$a' = a\left[1 - \exp\left(-\frac{1}{a}\right)\right] - 0.5\exp\left(-\frac{1}{2a}\right) \tag{8a}$$

where α is the Fourier number of the process defined as:

$$\alpha = \frac{D_S\, t_{SL}}{x^2} \tag{8b}$$

where t_{SL} is the time that the alloy spends in the semisolid state during both solidification and reheating, D_s is the diffusion coefficient of the solute in the solid state and x is the characteristic distance for back diffusion. In the case of equiaxed microstructures, this characteristic distance is half the grain size, $(d/2)$, while in dendritic microstructures, it is half the secondary dendritic arm spacing, (SDAS/2), as it evolves during ripening. The Fourier number, α, may vary from 0 (maximum microsegregation - Scheil equation) to ∞ (equilibrium solidification - lever rule), while the modified Fourier number, α', varies from 0 to 0.5 under the same conditions [18].

For a given alloy system, high cooling rates during solidification reduce the local solidification time, increasing the amount of residual non-equilibrium eutectic and reducing the degree of homogenization. At the same time, short solidification times result in a small grain size which represents the characteristic length for back diffusion, so higher cooling rates decrease the characteristic diffusion distance, decreasing the required homogenization time. The net effect of cooling rate, $\dot{T}$, on the Fourier number is (Appendix I):

$$\alpha \propto \dot{T}^{-1/3} \tag{9}$$

Therefore, the Fourier number decreases with the increase of the cooling rate, indicating that the conditions

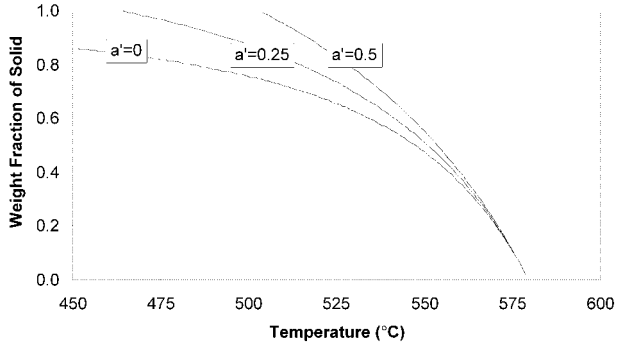

Figure 2 Evolution of weight fraction of solid with temperature in the Al-13wt.%Mg alloy, as calculated using: the phase diagram (equilibrium conditions, $a' = 0.5$), the Scheil model (maximum microsegregation, $a' = 0$), and Equation 7 for $a' = 0.25$ (partial homogenization).

prevailing during solidification, and therefore the process used to produce the alloy, affect the evolution of the solid content during subsequent remelting. As an example, Fig. 2 shows the effect of Fourier number on the evolution of weight fraction of solid in the Al-13wt.%Mg alloy.

In the thixoforming mode of semisolid processing, a reheating stage in the semisolid regime proceeds forming, and may affect the degree of microsegregation, and in turn, the solid content during forming. For example, current industrial practice involves the rapid heating, of the order of 170 K/min, of A356 Al-Si alloys from room temperature to forming temperatures above the eutectic within 200 s [27]. This heating rate is so high that homogenization and dissolution of non-equilibrium eutectic via solution treatment in the solid state are negligible[¶]. In this case, the degree of microsegregation is not expected to change while the alloy is still in the solid state. As a result, non-equilibrium liquid is formed as soon as the temperature exceeds the non-equilibrium eutectic temperature by melting microsegregated species that have resulted from prior non-equilibrium solidification conditions. It is also common practice to soak the alloys at the forming temperature in order to promote spheroidization and achieve a uniform distribution of the liquid phase. Significant homogenization may occur during that stage, depending on the alloy system and grain size, reducing the liquid content as a result of freezing of non-equilibrium liquid. Examples of homogenization times for various binary alloy systems with a near-equiaxed microstructure can be found in [29].

Non-equilibrium liquid can also form from melting homogenized and equilibrium microstructures. For example, at room temperature the Al-4wt.%Cu alloy consists of a solid solution of Cu in Al (α phase) and particles of θ phase. When the alloy is heated slowly, θ phase begins to dissolve, and if heating is slow enough, all the θ phase is dissolved above the solvus temperature. On the other hand, when the heating rate is high, much of the θ phase remains undissolved [30], and when the eutectic temperature of 548°C is reached, melting begins at the interface between the α phase and the θ phase forming non-equilibrium liquid.

This discussion shows clearly that, thermodynamic databases can be used to establish accurately the evolution of the solid content during melting if the alloy is near equilibrium, or in conjunction with an appropriate model that accounts for the thermal history of the alloy. Therefore, there is a need for experimental methods that evaluate directly the alloy on thermal conditions similar to the conditions employed by industrial practice. Nevertheless, the use of thermodynamic databases offers a very significant and unique advantage compared with all other methods. This method is a valuable tool for material selection and alloy design. For example, it allows for the evaluation of the sensitivity of the volume fraction of solid to minor temperature variations. For practical reasons this parameter must be small to ensure processability via the semisolid route [29]. Using thermodynamic database software, alloys with low sensitivity of the solid content to minor variations of temperature can be identified and new alloys can be designed.

3.2. Thermal analysis technique

The thermal analysis approach, specifically the method of partial areas, is approximate. As the temperature increases, the composition of the solid phase changes to maintain local equilibrium at the solid-liquid interface following the equilibrium phase diagram. More importantly, the heat of melting, which reflects the energy required by the atoms to be transferred from the solid phase to the liquid across the solid-liquid interface, is also a function of composition as it depends on the type of atoms, their concentration and their spatial distribution. A detailed examination, based on simple thermodynamic principles, that quantifies the effect of composition on the heat of solidification/melting shows that, there are significant errors in the results calculated by the method of partial areas, when the heat of melting of the alloy is significantly different from the latent heat of the solvent metal, i.e. when the alloy is not dilute. In addition, the error increases at medium solid content, which is the range of interest for semisolid processing. For example, the maximum error predicted for the Al-4wt.%Cu alloy is 0.02 at $f_s = 0.85$, while for the Al-17Si-4.5Cu alloy the error is 0.2 at $f_s = 0.07$ [31].

The use of thermal analysis techniques has an additional shortcoming. A comparison between the high heating rates used in semisolid processing (170 K/min) and the slow rates used in the DSC tests (5–30 K/min) shows that, current thermal analysis techniques do not simulate accurately industrial conditions as they cannot achieve very high heating rates. Homogenization is enhanced during measurements by thermal analysis, thus imposing an additional error on the results, due to the different thermal histories. This is very important for binary alloys, while conventionally cast commercial alloys with multiple alloying elements may exhibit slower homogenization rates than binary alloys.

[¶] In general, solution treatment is a very slow process, even at elevated temperatures. Based on [28], if a 40 μm grain is considered that contains 10 vol.% non equilibrium eutectic, uniformly distributed around its surface, the time required to dissolve 10 vol.% of the eutectic is 24 min for the Al-Cu system. This result shows that, the times required for solution treatment exceed the times used in semisolid processing, so no such change should be expected during the process.

Although thermal analysis may not portray accurately the evolution of the solid content during melting, it can provide useful information on characteristic temperatures such as the liquidus and solidus or eutectic, which can be used to identify the presence of non-equilibrium species in an alloy. These measurements may be performed either during cooling, to study the kinetics of solidification, or during heating to study the kinetics of melting, as it is described herein. The proper heating profile is dictated by the purpose of the experiment. For the study of casting processes, experiments should be performed during solidification. To get useful results, suitable for evaluating the solid content during thixoforming, experiments performed during cooling are inappropriate as they include nucleation effects and undercooling of the liquid phase. On the other hand, the study of the behavior of alloys during melting simulates more closely industrial conditions and avoids the problems of nucleation and undercooling, since overheating in metallic solids is always absent [32].

More importantly, thermal analysis can be used to compare the melting kinetics of similar alloys and provide with comparative information that otherwise would not be possible to obtain. Two examples follow that outline this advantage:

The first example shows the difference in the evolution of solid content during melting, between spray-cast and conventionally cast Al-4wt.%Cu alloys. Initially, a sample from spray-cast Al-4wt.%Cu alloy was examined. The melted sample was resolidified with a cooling rate of 100 K/min inside the DSC simulating conventional solidification conditions, and was tested again. The resulting DSC curves are shown in Fig. 3a. The difference between the two alloys lies in the presence of an endothermic reaction at 548°C for the conventionally solidified alloy, the eutectic temperature of the Al-Cu system. This reaction corresponds to the melting of non-equilibrium eutectic that has resulted from the non-equilibrium conventional solidification conditions. On the other hand, the spray-cast alloy does not exhibit such a reaction, and the temperature where heat starts to be absorbed for melting, that is indicated by the temperature where the DSC curve deviates from the baseline, coincides with the solidus temperature of the alloy, as predicted by the equilibrium phase diagram for the Al-4wt.%Cu alloy composition. This result agrees with our results from other spray-cast alloys and shows that, spray-cast microstructures are fully homogenized, and therefore, the evolution of the solid content in spray-cast alloys is more accurately predicted by using the phase diagram than by using the Scheil equation as has been proposed by other investigators for alloys in general [3, 33]. The results from the DSC, as well as the predictions of the lever rule and the Scheil equation that correspond to the Al-4wt.%Cu alloy composition, are shown in Fig. 3b. The observation that, the result of the thermal analysis for the spray-cast alloy is very close to the result predicted by using the lever rule shows that, the error imposed by using the method of partial areas is not significant, at least in this case where the Cu concentration is low. Microsegregation in spray-cast microstructures is often absent due to rapid solidification. That is because, liquid droplets experience significant

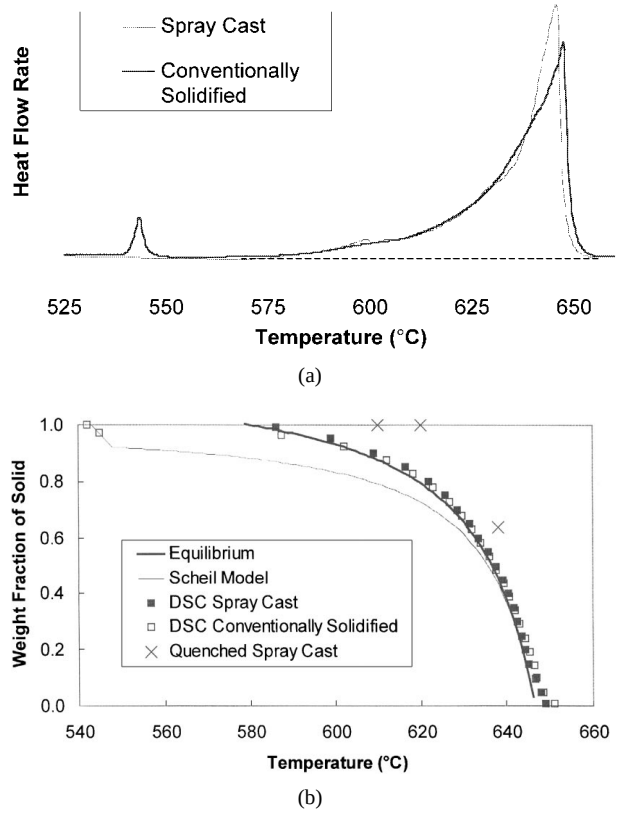

Figure 3 (a) DSC curves for Al-4wt.%Cu alloys produced by spray casting and under conventional solidification conditions; (b) evolution of weight fraction of solid as calculated using the lever rule, the Scheil equation and the method of partial areas for the Al-4wt.%Cu alloy. The results from the quenching experiments are superimposed.

undercooling [34], due to the high cooling rates during atomization (of the order of 10^3–10^5 K/s). In consequence, the solid that is formed inside the droplets has a composition that is closer to the nominal alloy composition than in typical castings. Furthermore, the solid content of the spray prior to deposition (which is of the order of 50 vol.%) homogenizes quickly due to the very small droplet size and the small SDAS within the droplets. After deposition, solidification continues at a relatively low cooling rate (1–20 K/s), completing homogenization.

The second example shows the difference in the kinetics of melting between spray-cast, SIMA and MHD-cast Al-7wt.%Si alloys. The weight fraction vs. temperature curves, calculated using the method of partial areas, are shown in Fig. 4. In the same figure, the predictions of the lever rule for the Al-7wt.%Si alloy composition are also shown. It is interesting to observe that, the three alloys follow different melting patterns. At any temperature below 590°C, where the melting of the eutectic is complete, the MHD-cast alloy shows the lowest amount of solid phase, while the spray-cast alloy the highest. These differences are attributed to the following factors:

- the MHD-cast alloy contains 0.3% Mg, while Mg is absent in the SIMA and spray-cast alloys. The presence of Mg in the MHD-cast alloy shifts the eutectic temperature approx. 8°C lower than in the spray-cast and SIMA alloys, so melting

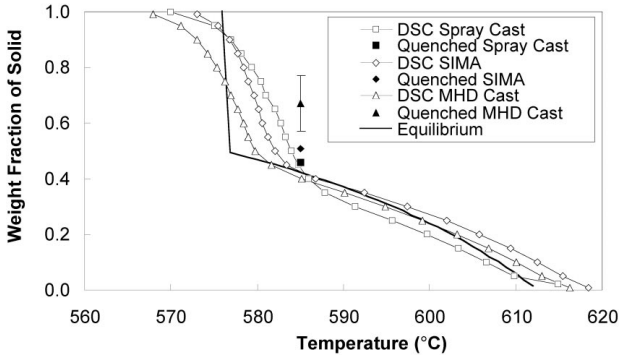

Figure 4 Evolution of weight fraction of solid for Al-7wt.%Si alloys produced by spray casting, SIMA and MHD casting, as measured using DSC. The results from the quenching experiments for these alloys and the predictions of the phase diagram for the same alloy composition are also shown.

starts earlier producing Mg-rich liquid. In addition, the typical cooling rates during solidification of MHD-cast alloys (6–10 K/s) [35] are higher than in SIMA [12], therefore, the amount of non-equilibrium species due to microsegregation is also higher in the MHD-cast alloy than in the SIMA alloy.

- While SIMA and spray-cast alloys have the same chemical composition, SIMA shows a higher liquid content at any temperature compared with the spray-cast alloy, due to:

  i. the presence of microsegregated species, a result of conventional solidification conditions [36], and,
  ii. the modification of the Al-Si phase diagram that the spray-cast alloy follows, as the result of the very high cooling rates during spray deposition, that increase the eutectic composition in the Al-Si system and the maximum solute solubility of Si the Al, thus decreasing the amount of eutectic formed, changing the kinetics of melting [37, 38].

In conclusion, thermal analysis techniques may be occasionally inaccurate, but the error is small for dilute alloys. Even when the error is significant, thermal analysis techniques can provide information on differences in the melting kinetics, helping us understand the effects of microstructure, as resulted from the prior thermal conditions. Such an insight cannot be provided using any other technique. Therefore, by using thermal analysis techniques, thermal information is related directly to the physical picture of the microstructure of the alloy as it melts, and valuable information on the solidification process that produced these microstructures can be obtained.

3.3. Image analysis in samples quenched from the semisolid state

Attempts to quench alloys with a high solid content (<75 vol.%) and consist mainly of a single phase (spray-cast 2014 and Al-4wt.%Cu) failed to reveal the presence of liquid. This is attributed to insufficient cooling rates. At high volume fractions of solid, liquid wets the grain boundaries by forming a thin film that solidifies almost instantly. For example, if it is assumed that a spherical grain, 50 μm in diameter, is totally surrounded by liquid, the average thickness of the liquid film, t, is only 1.8 μm, at volume of liquid, g_L, of 20 vol.%. This thickness is given by:

$$t = \frac{d}{2}\left(1 - (g_L)^{1/3}\right) \tag{10}$$

The quenching experiments do, however, reveal the presence of liquid at medium and low volume contents of solid. Fig. 5 shows typical microstructures of spray-cast 2014 and Al-4wt.%Cu at 25 vol.% and 50 vol.% solid respectively, while Fig. 6 shows micrographs from the quenched microstructure obtained from Al-7wt.%Si alloys quenched at 55 vol.% liquid. While the darker regions in the micrographs consist of very fine dendrites and/or eutectic, resulting from rapid solidification of the liquid phase, the white areas correspond to the solid phase.

Morphological instability in the Al-7wt.%Si alloys at the solid-liquid interface during rapid solidification led to dendritic growth from the surface of the solid grains that has to be taken into account during the measurement of the solid phase (Fig. 6b). These fine dendrites can be excluded manually when the microstructure is observed at high magnification so the original solid-liquid interface can be detected. Nevertheless, image analysis cannot be performed accurately at such

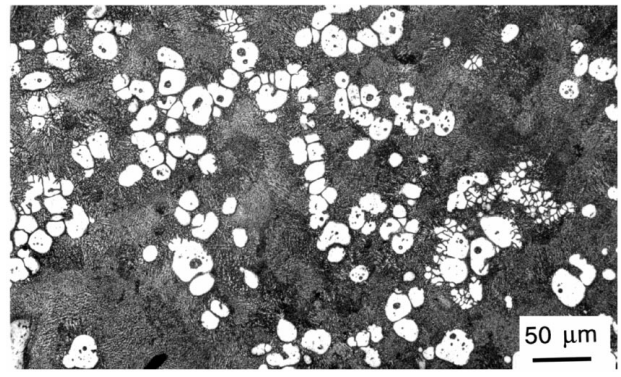

(a)

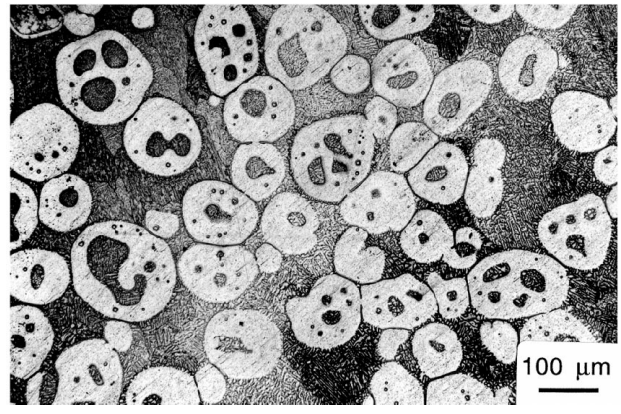

(b)

Figure 5 Microstructure of Al-Cu alloys quenched from the semisolid state: (a) 2014 with 25 vol.% solid; (b) Al-4wt.%Cu with 50 vol.% solid.

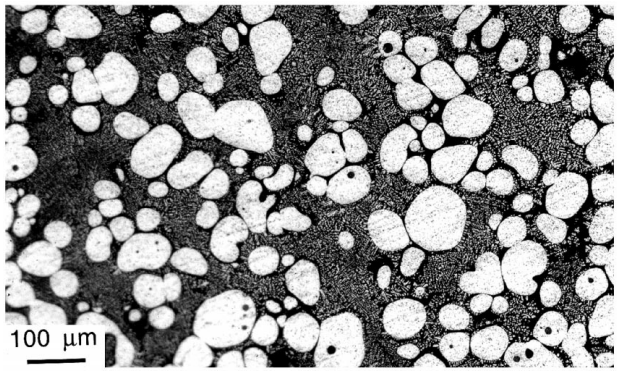

(a)

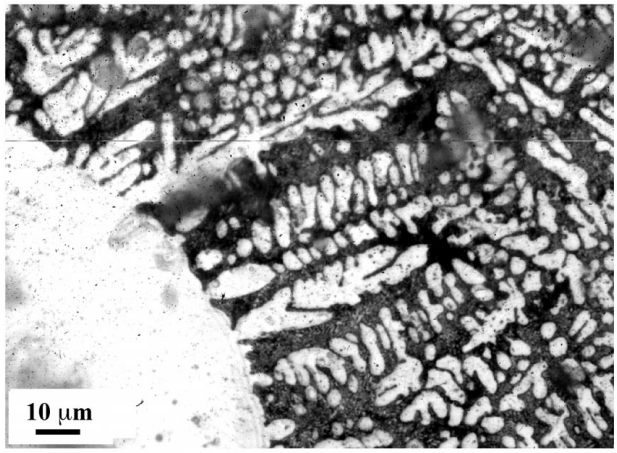

(b)

Figure 6 Microstructure of Al-7wt.%Si alloys quenched from the semisolid state: (a) spray-cast alloy with 55 vol.% solid; (b) dendritic growth on the surface of rapidly solidified semisolid SIMA Al-7wt.%Si.

high magnifications where the eutectic is resolved. In this case, thresholding will separate the components of the eutectic instead of considering it as a single phase (liquid). Furthermore, a compromise in magnification, where image analysis is performed, is essential. While high magnification offers the advantage of high resolution, it minimizes the measured area and increases the risk of bad image quality due to inaccurate focusing. On the other hand, low magnification increases significantly the area covered by every micrograph, thus minimizing the error due to inhomogeneous distribution of phases, but decreases the resolution of the image.

In most cases during our experiments, the volume fraction of solid was overestimated, compared with the predictions of the lever rule for the nominal alloy composition, and the thermal analysis. The results from the quenching experiments are superimposed in Figs 3b and 4 for the Al-4wt.%Cu and Al-7wt.%Si alloys respectively. This overestimation is so significant to be attributed to errors in thermal analysis and in the use of phase diagrams, and found to be more severe in practically single phase Al-Cu alloys (Al-4wt.%Cu and 2014) compared with two-phase Al-Si eutectic alloys. Similar results that exhibit such an overestimation of the volume fraction of solid have been reported by other investigators [15, 39].

This overestimation of the solid content must be attributed to the insufficient cooling rates. During quenching, growth is constrained by the temperature profile in the liquid phase. Furthermore, it is expected that any instabilities that lead to dendritic growth become dominant after the initial solid-liquid interface has moved by epitaxial planar solidification by a distance of the order of the secondary arm spacing, as dictated by the local cooling rate. A correction procedure can be applied, based on the secondary dendrite arm spacing (SDAS) in the rapidly solidified eutectic (see Appendix II):

$$\delta g_S \leq g_S\left(6\frac{\mathrm{SDAS}}{d}\right) \tag{11}$$

where δg_S is the difference between the experimentally measured and the actual volume fraction of solid, and d is the grain size in the semisolid state. The results, when corrected using Equation 11, are in good agreement with the results from the DSC and the predictions of the phase diagram. For example, spray-cast Al-4wt.%Cu alloys quenched from 638°C show 64 vol.% solid (Fig. 3b). Using Equation 11, the calculated value for δg_S is 22 vol.% and therefore, the 'corrected' value of g_s is 42 vol.%. At the same temperature, the solid content predicted by DSC and the use of phase diagram is 46 vol.%.

Based on Equation 11, the magnitude of the error is significant when the solid grain size is small with respect to the achieved SDAS. Therefore, the local cooling rate dictates the amount of epitaxially solidified liquid alloy and thus, the overestimation of the volume fraction of solid.

Obviously, two-phase eutectic alloys reveal the eutectic content that is in liquid form in the semisolid state, but even in this case, the eutectic content measured in MHD-cast A356 is less compared with the amount of eutectic measured in spray-cast and SIMA Al-Si alloys, examined under similar conditions. This difference is attributed to the morphology and distribution of the solid phase and the eutectic. The eutectic may be in divorced form, so the amount of visible eutectic is reduced. In addition, the solid phase in MHD-cast alloys is closely spaced, while in SIMA and spray-cast alloys, the solid phase is dispersed into the liquid matrix. As a result, for a given cooling rate and therefore the same amount of epitaxially solidified alloy, space of liquid fills more in MHD-cast alloys than in SIMA and spray-cast alloys.

Another parameter that affects the local temperature field, besides the thermal properties of the sample and the quencher and the thermal conditions of the experiment (i.e. the heat transfer coefficient between the quencher and the sample) is the dimensions of the sample. In our experiments, the thickness of the samples was kept to minimum (2 mm) but as the discussion showed, it was found insufficient to permit fast-enough cooling rates. The effect of the thickness of the sample on the amount of liquid that freezes epitaxially on the solid grains, was determined by a modified quenching experiment. A specimen of spray-cast 2014 was quenched from a temperature of 630°C without the presence of the copper weight that is required to

drag it into the quencher. As a result, only one surface of the sample was in direct contact with the quencher and locally, it was quenched instantly, while the alloy experienced decreasing cooling rates at distances away from the quencher-sample interface. At a distance of 2 mm away from the rapidly quenched surface of the sample, the measured volume fraction of solid increased twofold (Fig. 7a). An analysis that appears in Appendix II shows the strong dependence of the error in measuring the volume fraction of solid with distance from the quencher-sample interface, x:

$$\frac{g_{s(exp)} - g_s}{g_s} \propto x^{2/3} \tag{12}$$

where $g_{s(exp)}$ is the measured volume fraction of solid.

This analysis shows that, errors using this method are unavoidable. Additional disadvantages of this method are the complexity in optimization and setup of the experiment and its labor-consuming character. Nevertheless, the volume fraction of solid may be estimated by extrapolating the experimentally determined values of volume fraction of solid as a function of distance from the quenched interface, based on an acceptable model. Based on the model developed in Appendix II, Equation 12 becomes:

$$\frac{g_{s(exp)}}{g_s} = 1 - Ax^{2/3} \Leftrightarrow g_{s(exp)} = g_s + Bx^{2/3} \tag{13}$$

where A and B are constants. This model was applied to the results of our experiment, as they appear in Fig. 7b,

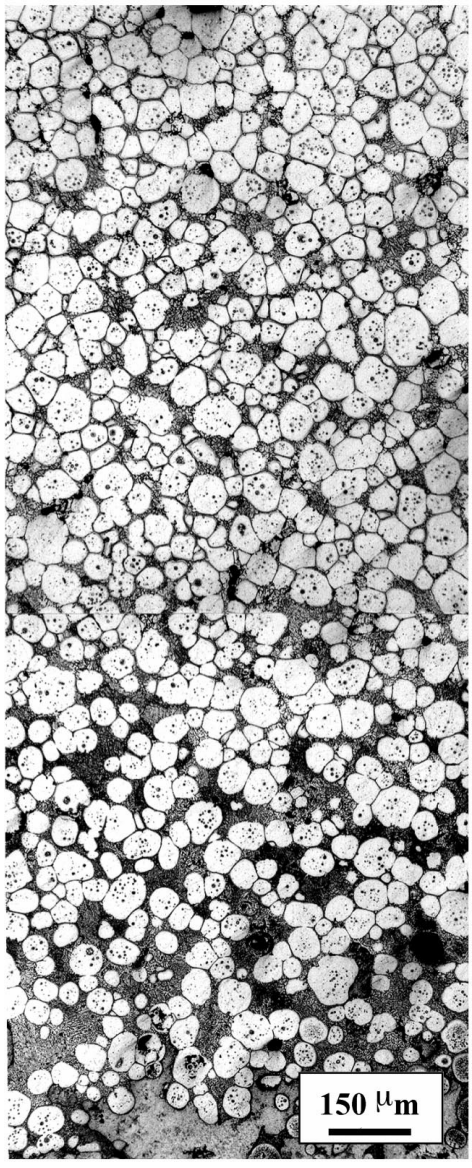

(a)

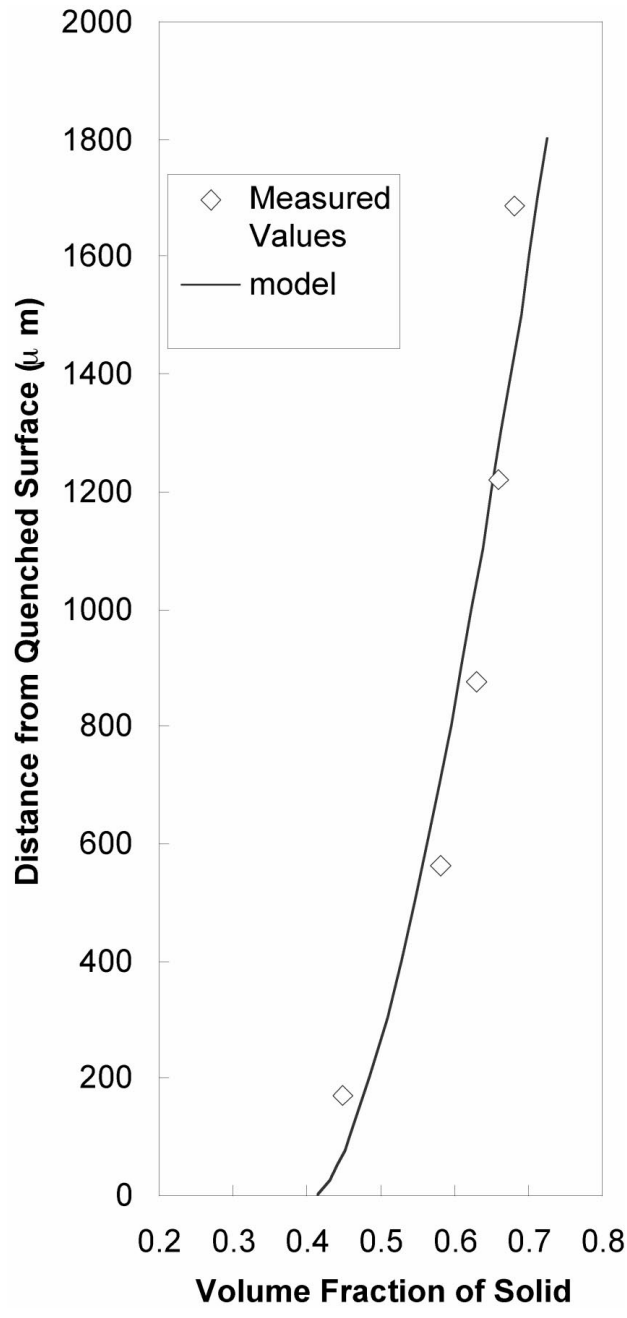

(b)

Figure 7 Change of solid content with distance from the quenched surface in spray-cast 2014 soaked at 630°C for 2 min: (a) microstructure; (b) image analysis measurements and model predictions.

and yielded a value of 0.42 for the g_s, while the DSC calculated a value of 0.39 for the same alloy at 630°C, the quenching temperature.

The method, besides its use for the measurement of the volume fraction of solid, offers a very significant advantage: it reveals the microstructure in the semisolid state (morphology of the solid phase, distribution of phases) providing with very valuable information that can be used to characterize the evolution of microstructure and rheological behavior of alloys in the semisolid state [11].

4. Conclusions

The evaluation of the methods that are used to determine the evolution of the volume fraction of solid as a function of temperature in the semisolid state (use of thermodynamic data, thermal analysis techniques, and quantitative metallography after quenching experiments) showed that:

- all methods are approximate
- the use of thermodynamic data can predict the maximum range where the volume fraction of solid may vary as a function of temperature, but requires additional information in order to take into account the thermal history of the alloy
- DSC results may include an error due to the approximation of the partial areas method that depends on the composition of the alloy. Nevertheless, the error is very small in commonly used dilute alloys, making this method attractive due to minimal specimen preparation required. Another restriction is the low heating rates used in DSC, compared with the fast heating rates that are used in industrial applications of semisolid processing.
- use of image analysis after quenching provides useful results, provided that, the quenching conditions and specimen dimensions are properly chosen and the necessary corrections are applied to the results.
- All three methods have significant and unique advantages. The use of thermodynamic data is a fast and reliable tool for alloy design, thermal analysis provides with comparative information and reveals the prior thermal history of an alloy, and, image analysis after quenching reveals the morphology of microstructure in the semisolid state.

Appendix I

In general, the characteristic diffusion distance, x, (grain size, d, or secondary dendrite arm spacing, SDAS) scales with the local solidification time, t_f [18, 25]:

$$x \propto t_f^{1/3} \tag{A.1}$$

Therefore, the Fourier number becomes:

$$\alpha = A' \frac{D_s t_f}{\left(t_f^{1/3}\right)^2} \Leftrightarrow \alpha \propto t_f^{1/3} \tag{A.2}$$

where A' is a constant. For a fixed solidification range, ΔT:

$$\dot{T} = \frac{\Delta T}{t_f} \Leftrightarrow t_f \propto (\dot{T})^{-1} \tag{A.3}$$

Combining Equations A.2 and A.3 we obtain Equation 9.

Appendix II

The transient thermal conditions within a quenched specimen may be described by assuming that the sample behaves as a semi-infinite medium that is initially at a uniform temperature T_i, and at time $t=0$ one of its surfaces is quenched to a temperature T_S, as the modified experiment describes. If it is also assumed that the heat flux is one-dimensional then, the temperature profile within the sample is given as a function of time, t, and position, x, away from the quenched interface by [40]:

$$\frac{T - T_S}{T_i - T_S} = \mathrm{erf}\left(\frac{x}{2\sqrt{\alpha t}}\right) \tag{A.4}$$

where α is the Fourier number of the sample, defined as:

$$\alpha = \frac{kt}{\rho C_p x^2}$$

where k, ρ and C_p are the thermal conductivity, density and heat capacity of the sample respectively*. If it is assumed that the sample solidifies in a non-equilibrium manner then, the solidification range during quenching is bound by T_i and T_E, the eutectic temperature. Therefore the local solidification time, t_f, can be calculated using Equation A.4:

$$t_f = \frac{x^2}{4\alpha\left[\mathrm{erf}^{-1}\left(\frac{T_E - T_S}{T_i - T_S}\right)\right]^2} \Leftrightarrow t_f \propto x^2 \tag{A.5}$$

The thickness of epitaxially solidified alloy, ΔR, is of the order of the secondary dendritic arm spacing that is related to t_f by Equation A.1. Combining Equations A.1 and A.5:

$$\Delta R \propto x^{2/3} \tag{A.6}$$

The error due to the epitaxial layer solidifying on the solid grains is given by:

* In general, k, C_p and ρ should account for the presence of both the solid and liquid phases in the sample by using a rule of mixture. Since growth is extremely fast and epitaxial growth occurs at the very early stages of solidification, then it may be assumed that k, C_p and ρ_s are not functions of g_s and may be considered as constants, retaining their initial value.

$$\frac{\delta g_S}{g_S} = \frac{(\chi_{WS} V_{\text{epitaxial layer}})/V_{\text{total}}}{V_{\text{solid grain}}/V_{\text{total}}} = \chi_{WS} \frac{V_{\text{epitaxial layer}}}{V_{\text{solid grain}}} \tag{A.7}$$

where χ_{WS} is the fraction of the surface of the solid grain that is wetted (usually close to 1). If R is the radius of the solid grain in the semisolid state then, Equation A.7 becomes:

$$\frac{\delta g_S}{g_S} = \chi_{WS} \frac{4/3\pi(R + \Delta R)^3 - 4/3\pi R^3}{4/3\pi R^3}$$
$$= \chi_{WS} \left[\left(1 + \frac{\Delta R}{R} \right)^3 - 1 \right] \tag{A.8}$$

Finally, when ΔR is small compared with the grain size d, and of the order of the SDAS, then:

$$\frac{\delta g_S}{g_S} = 6\chi_{WS} \frac{\Delta R}{d} \leq 6 \frac{\text{SDAS}}{d} \tag{A.9}$$

Combining Equations A.6 and A.9 we obtain Equation 12.

Acknowledgements

Support for this work was provided by the Civil and Mechanical Systems Division of the National Science Foundation (Grant No. MSS-9313254). Material has been provided by Osprey Metals Ltd., Neath, U.K., and CTC, Johnstown, PA, USA. Stimulating discussions with Professor Roger D. Doherty are gratefully acknowledged.

References

1. M. C. FLEMINGS, *Metall. Trans.* **21A** (1991) 957.
2. D. H. KIRKWOOD, *Int. Mater. Rev.* **39**(5) (1994) 173.
3. P. A. JOLY and R. MEHRABIAN, *J. Mater. Sci.* **11** (1976) 1393.
4. C. P. CHEN and C. Y. CHAO, *Acta Mater.* **45**(5) (1997) 1955.
5. E. TZIMAS and A. ZAVALIANGOS, *ibid.* **47**(2) (1999) 517.
6. S. C. HARDY and P. W. VOORHES, *Metall. Trans.* **19A** (1988) 2713.
7. C. L. MARTIN, S. B. BROWN, D. FAVIER and M. SUERY, *Mater. Sci. Engng.* **A202** (1995) 112.
8. L. SALVO, W. R. LOUE and M. SUERY, *ISIJ Intl.* **35** (1995) 798.
9. W. R. LOUE and M. SUERY, *Mat. Sci. Engng.* **A203** (1995) 1.
10. S. BLAIZ, W. LOUE and C. PLUCHON, in Proceedings of the 4th Int. Conf. on the Processing of Semi-Solid Alloys and Composites, Sheffield, UK, June 1996, edited by D. H. Kirkwood and P. Kapranos (The University of Sheffield, Sheffield, 1996) p. 187.
11. E. TZIMAS and A. ZAVALIANGOS, *Mater. Sci. Engng. A*, in press.
12. E. TZIMAS, PhD thesis, Drexel University, Philadelphia, PA, USA, 1997.
13. P. S. GRANT, R. P. UNDERHILL, W. T. KIM, K. P. MINGARD and B. CANTOR, in Proceedings of the 2nd International Conference on Spray Forming, Swansea, UK, 1993, edited by J. V. Wood (Woodhead Publishing, Cambridge, UK, 1993) p. 45.
14. R. P. UNDERHILL, P. S. GRANT, D. J. BRYANT and B. CANTOR, *J. Mat. Syn. Proc.* **3**(3) (1995) 171.
15. S.-W. CHEN and C.-C. HUANG, *Acta Mater.* **44**(5) (1996) 1955.
16. S.-W. CHEN and C.-J. JENG, *Metall. Mater. Trans. A* **27A** (1996) 2722.
17. S.-C. JENG and S.-W. CHEN, *Acta Mater.* **45**(12) (1997) 4887.
18. W. KURZ and D. J. FISCHER, "Fundamentals of Solidification," 3rd ed. (Trans Tech Publications, Switzerland, 1989).
19. H. FREDRIKSSON, "Metals Handbook, Vol. 15," 9th ed. (ASM Intl., Metals Park, Ohio, 1985) p. 182.
20. J. L. MCNAUGHTON and C. T. MORTIMER "Differential Scanning Calorimetry Vol. 10," IRS : Physical Chemistry Series 2 (Butterworths, London, 1975).
21. G. F. VANDER VOORT, "Metals Handbook, Vol. 10," 9th ed. (ASM Intl., Metals Park, Ohio, 1985) p. 309.
22. R. E. SPEAR and G. R. GARDNER, *Trans. AFS* **71** (1963) 209.
23. T. F. BOWER, H. D. BRODY and M. C. FLEMINGS, *Trans. AIME* **236** (1966) 624.
24. U.S. National Institutes of Health: http://rsb.info.nih.gov/nih-image/
25. M. C. FLEMINGS, "Solidification Processing" (McGraw Hill, N.Y., 1974).
26. THERMOCALC, TCAB, Stockholm, Sweden.
27. ALUMINIUM PECHINEY, Althix Billets, Information Pamphlet, April 1996.
28. S. N. SINGH and M. C. FLEMINGS, *Trans. AIME* **245** (1969) 1803.
29. E. TZIMAS and A. ZAVALIANGOS, *Mater. Manuf. Proc.* **14**(2) (1999) 217.
30. H. B. AARON and G. R. KOTLER, *Metall. Trans.* **2** (1971) 393.
31. A. ZAVALIANGOS and E. TZIMAS, *Metall. Trans. B*, in press.
32. D. P. WOODRUFF, "The Solid-Liquid Interface" (Cambridge University Press, Cambridge, England, 1973).
33. D. B. SPENCER, R. MEHRABIAN and M. C. FLEMINGS, *Metall. Trans.* **3** (1972) 1925.
34. P. MATHUR, D. APELIAN and A. LAWLEY, *Acta Metall.* **37**(2) (1989) 429.
35. W. KAHRMANN, R. SCHRANGER and K. YOUNG, *ibid.* **10** 154.
36. K. P. YOUNG, C. P. KYONKA and F. COURTOIS, U.S. Patent 4,415,374 (1983).
37. L. F. MONDOLFO, "Aluminum Alloys: Structure and Properties" (Butterworth, London, 1979).
38. S. SU, X. LIANG, A. MORAN and E. J. LAVERNIA, *Int. J. Rapid Solid.* **8** (1994) 161.
39. M. C. FLEMINGS, "TMS, in Light Metals 1998," edited by B. Welch (TMS, Warrandale, PA, 1998) p. 1103.
40. D. R. POIRIER and G. H. GEIGER, "Transport Phenomena in Materials Processing" (TMS, Warrendale, PA, 1994).

Received 15 September 1999
and accepted 4 April 2000